JOURNAL OF SOLID STATE CHEMISTRY 119, 311–318 (1995)

An Electron Diffraction Study of the Type II $Bi_{2-x}Nb_xO_{3+x}$ Solid Solution

D. Tang*,[1] and W. Zhou†,[2]

*Department of Chemistry, University of Cambridge, Lensfield Road, Cambridge CB2 1EW, United Kingdom; and †IRC in Superconductivity, University of Cambridge, Madingley Road, Cambridge CB3 0HE, United Kingdom

Received March 21, 1995; accepted May 25, 1995

The structural chemistry of the type II $Bi_{2-x}Nb_xO_{3+x}$ solid solution has been studied via computer simulation of the electron diffraction patterns. The Nb cations were found to exist in some Nb_7O_{30} and $Nb_{18}O_{72}$ clusters which were in partially ordered arrangements in the δ-Bi_2O_3 matrix, forming some incommensurate superstructures. Commensurate 11 × 11 × 11 superstructures in $Bi_{17}Nb_3O_{33}$, Bi_9NbO_{16}, and an 8 × 8 × 8 superstructure in $Bi_4NbO_{8.5}$ derived from the δ-Bi_2O_3 subcell have been proposed in order to approach the real structures. © 1995 Academic Press, Inc.

INTRODUCTION

Pure Bi_2O_3 has been known to exist in four phases at different temperatures, i.e. α-phase (1) at room temperature, δ-phase (1) above 729°C, and two intermediate phases, β- (2) and γ-Bi_2O_3 (1). The most attractive one of these modifications is perhaps the δ-Bi_2O_3, which has a defect fluorite structure containing 25% oxygen vacancies and is the best oxide ion conductor known (3). However, this phase cannnot be quenched to room temperature unless other metal oxides are added to form δ-Bi_2O_3-related solid solutions.

The structural chemistry of these solid solutions is much more complicated than that we observed in X-ray powder diffraction (XRD) studies (4), from which only the information of the δ-Bi_2O_3-like basic structure can be obtained. For example, the Nb-doped δ-Bi_2O_3 solid solution, $Bi_{2-x}Nb_xO_{3+x}$, was reinvestigated previously (5, 6) using high resolution electron microscopy (HREM) and several types of superstructures were revealed. When $x \leq 2/17$, all the Nb cations existed in isolated but ordered NbO_6 octahedral units forming a 2 × 2 × 2 body-centred cubic supercell based on the δ-Bi_2O_3 subcell, designated a type I superstructure. When $1/10 \leq x \leq 7/15$, a type II superstructure was observed, in which each four NbO_6 octahedra joined together to form a Nb_4O_{18} tetrahedral cluster. Every two Nb_4O_{18} clusters shared one Nb atom to form a "dumbbell"-like Nb_7O_{30} cluster. Some of these Nb_7O_{30} clusters might link each other to form an even larger cluster, "garland"-like $Nb_{18}O_{72}$. Further addition of Nb_2O_5 into the solid solution gave rise to a layered compound, type III $Bi_7Nb_3O_{18}$ (6) and an Aurivillius phase $Bi_5Nb_3O_{15}$ (7). Similar phenomena were also observed in the Bi_2O_3–V_2O_5 (8), Bi_2O_3–Ta_2O_5 (9), and Bi_2O_3–WO_3 (10) systems. Therefore, a multi-order approximation method has been introduced to describe the structures of these imperfect solid solutions; i.e., the δ-Bi_2O_3-like substructure (1) detected by XRD is the first-order approximation, and the various types of superstructures due to the cation ordering are the second-order approximations to the true structures of these materials.

The Nb-doped type I and type III superstructures mentioned above are commensurate and have been well determined using HREM. However, the type II superstructure in this ternary oxide system is incommensurate. The positions and intensities of the satellite electron diffraction spots were found to vary with the composition. In the previous report, only one model for this type of superstructure was proposed with a typical composition of $Bi_4NbO_{8.5}$ (5) based on computer image simulation methods. When the Nb content was reduced, contrast of the HREM images from these materials became very low so that it was impossible to confirm any model using the image simulation technique. The low image contrast resulted from the unusually large unit cells of these materials (e.g., 44 Å × 44 Å × 44 Å for $Bi_4NbO_{8.5}$) and from the complication of the structures, in which there were too many atoms superimposed on each other along any of the principal projections. Consequently, the image contrast became insensitive to a single atomic position within an atomic column.

[1] Present address: National Center for HREM, Laboratory of Materials Science, Delft University of Technology, Rotterdamseweg 137, 2628 AL Delft, The Netherlands.

[2] To whom correspondence should be addressed at Department of Chemistry, University of Cambridge, Lensfield Road, Cambridge CB2 1EW, United Kingdom

0022-4596/95 $12.00

The well-established HREM theories (11–13) give the electron microscopic image wavefunction as

$$\Psi_i(x, y) = F^{-1}(\Psi_d(u, v)H(u, v)).$$

Here (x, y) denotes two-dimensional coordinates in real space at a plane perpendicular to the incident electron beam, (u, v) the corresponding coordinates in a reciprocal space, Ψ_d the diffraction wavefunction, and $H(u, v)$ an aberration function. Multiplying $H(u, v)$ to the diffraction function reflects the imperfections of the electron optical system of a microscope. Unless $H(u, v)$ is a constant, which is never strictly true, one cannot have a HREM image identical to the projected structure.

However, the aberration function acts on a selected area electron diffraction (SAED) pattern much less than on the corresponding image. First, the recorded diffraction pattern is the modular square of the wavefunction. Two of the most important imperfections of a HREM image, the defect of focus (Δf) and spherical aberration of the objective lens (C_s), intend to introduce an extra phase into the wavefunction. This phase change of a complex function does not show up in a modular-square-map. Second, the effects of chromatic aberration and beam divergence due to instability of the electron beam, lens current, and the limited size of the source, which are expressed as the envelope function in $H(u, v)$ for a HREM image, actually only enlarge the diffraction spots. As long as the calculation of diffraction pattern is not strictly quantitative, nearly all the important image aberrations mentioned above are not necessary to be considered in the simulation of a SAED pattern. Therefore, simulation of SAED patterns provides a worthwhile alternative for solving a complex structure.

In this report, we present our investigation of the Nb-doped type II δ-Bi_2O_3 solid solutions by computer simulations of the experimentally observed SAED patterns.

EXPERIMENTAL

Polycrystalline specimens of $Bi_4NbO_{8.5}$, $Bi_{17}Nb_3O_{33}$, and Bi_9NbO_{16} were prepared by solid–solid reaction of Bi_2O_3 and Nb_2O_5. The details of preparation conditions were the same as those presented in the previous report (5). Homogeneities of the specimens were examined by XRD and later confirmed by energy-dispersive X-ray microanalysis (EDS) and SAED studies. The SAED patterns were obtained from a Jeol JEM-200CX electron microscope operating at 200 kV with a ±45° double tilt goniometer stage.

In order to calculate SAED patterns, a routine HREM image simulation program was split, and the intermediate wave function at the back focal plane was squared and plotted on a two dimensional diagram for comparison with the experimental patterns. The intensities of diffraction spots were represented by areas of circles, except for the central transmitted spot. A threshold coefficient P was introduced so that if the strongest amplitude (excluding the transmitted one) was in unity, spots would appear in the diagram only if they had amplitude greater than $1/P$. A trial and error method was used to select models to reproduce the experimental SAED patterns.

RESULTS AND DISCUSSION

$Bi_4NbO_{8.5}$

Many SAED patterns and HREM images viewed down the various directions have been obtained from $Bi_4NbO_{8.5}$. Those along the [110] and [100] directions are presented in Fig. 1. The HREM images were recorded on another Jeol JEM-200CX electron microscope with electron optical parameters $C_s = 1.2$ mm and $C_c = 1.4$ mm, corresponding to a point resolution at optimum focus of 2.43 Å. The main diffraction spots are indexed onto the δ-Bi_2O_3-like fluorite subcell. The satellite diffraction spots form very complicated patterns and it was found by measuring their positions that the superstructure must be incommensurate. In order to approach the real structure, the closest commensurate unit cell was chosen which had an 8 × 8 × 8 supercell derived from the δ-Bi_2O_3 subcell.

Suffering from multiple scattering problems, to deduce the space group of this structure from electron diffraction patterns is in some degree of risk. The first model for $Bi_4NbO_{8.5}$ was indeed built up initially by analyzing the HREM image as shown in Fig. 1a. As discussed in the previous report (5), the HREM images viewed down the ⟨110⟩ directions gave us the best picture to reveal the superstructure, since more details of the image contrast along these directions could be observed in comparison with other directions; e.g., the [100] direction as shown in Fig. 1b. The first stage of the logic of modeling this structure was as follows.

According to a laser Raman study performed by I. E. Wachs and his co-workers, all the Nb cations in the specimens were octahedrally coordinated by oxygen (14). The diamond-like pattern of lattice fringes visible in the image of Fig. 1a showed strong similarities to those observed in pyrochlore and its derivative structures (15) when viewed down the ⟨110⟩ directions. An 8 × 8 × 8 superstructure derived from δ-Bi_2O_3 was initially proposed by placing the NbO_6 octahedra in a pyrochlore-like arrangement to all the {111} planes of this supercell. Image simulations from this model reproduced the basic diamond-like contrast of the experimental images. But, they did not provide a correct representation of the detail within the diamond-shaped regions. In addition, the {111} planes consisting solely of NbO_6 octahedra not only contained too many Nb cations, but also raised strong lattice strain due to the

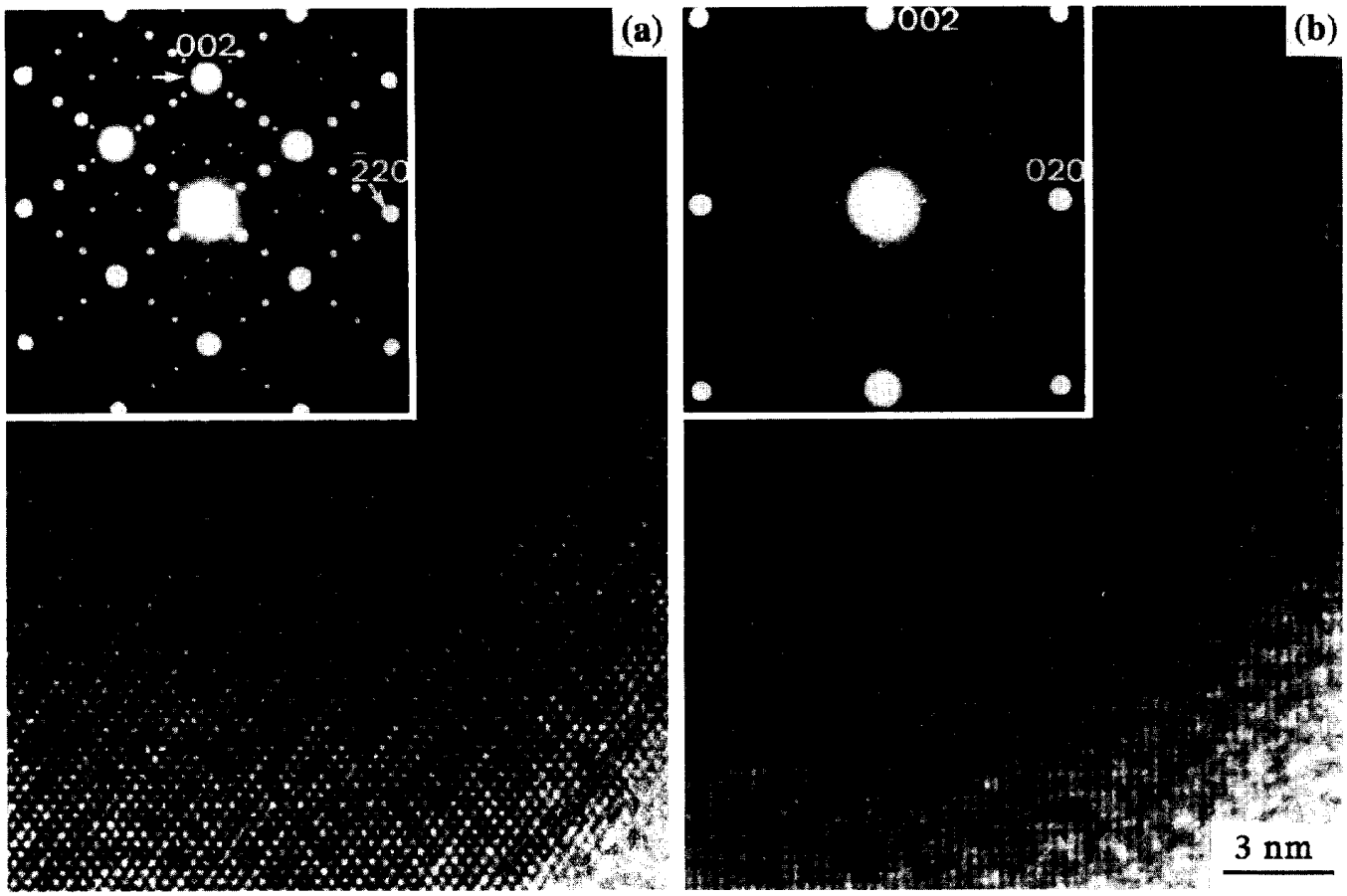

FIG. 1. SAED patterns and corresponding HREM images from $Bi_4NbO_{8.5}$, viewed down the (a) [110] and (b) [100] directions. The main diffraction spots are indexed onto the δ-Bi_2O_3-like subcell.

different properties between the chemical bonds of Bi–O and Nb–O. Consequently, some NbO_6 octahedra must be removed to break these {111} Nb–O planes into some Nb–O clusters. To do so, we have to consider the possible space groups implied by the SAED patterns.

Reviewing all the SAED patterns obtained from $Bi_4NbO_{8.5}$, the reflection conditions corresponding to the $8 \times 8 \times 8$ supercell seem to be

$$\begin{aligned} &h00, && h = 4n;\\ &hk0, && h, k = 2n, h + k = 4n;\\ &hhh, && h \neq 4;\\ &hhl, && h + l = 2n; \text{and}\\ &hkl, && h + k = 2n. \end{aligned}$$

The possible space group with the highest symmetry is therefore $Fd3m$ instead of $Fm3m$ for δ-Bi_2O_3. We then used this information to remove some NbO_6 octahedra from the {111} planes of the $8 \times 8 \times 8$ supercell. The final model contains Nb_7O_{30} and $Nb_{18}O_{72}$ clusters, all lying on the {111} planes with an arrangement as shown in Fig. 2. In detail, all the Nb cations in the Nb_7O_{30} clusters are located at (16 *c*) $\bar{3}$ *m* and (96 *g*) *m* (x, x, z = 1/16, 1/16, 2/16) and those forming the $Nb_{18}O_{72}$ clusters at (96 *g*) *m* (x, x, z = 1/16, 1/16, 12/16), (96 *g*) *m* (x, x, z = 2/16, 2/16, 8/16), and (96 *h*) 2 (x = 5/16) of space group $Fd3m$ with the origin at $\bar{4}3$ m.

Using this model, the HREM image in Fig. 1a has been successfully matched by computer image simulations in different areas with different specimen thicknesses and lens defocusses (5). However, the image matching for such a complicated structure judged by naked eyes still left some degree of speculation, especially at the thin area where the superstructural information was very limited. We could not be very much in certain about this model until the simulations of the SAED patterns were performed as presented in this report.

In the simulations of SAED patterns, an aliasing effect which introduces a fake periodicity in reciprocal space (16) must be considered. This effect becomes more prominent since the resolution of SAED simulation is much

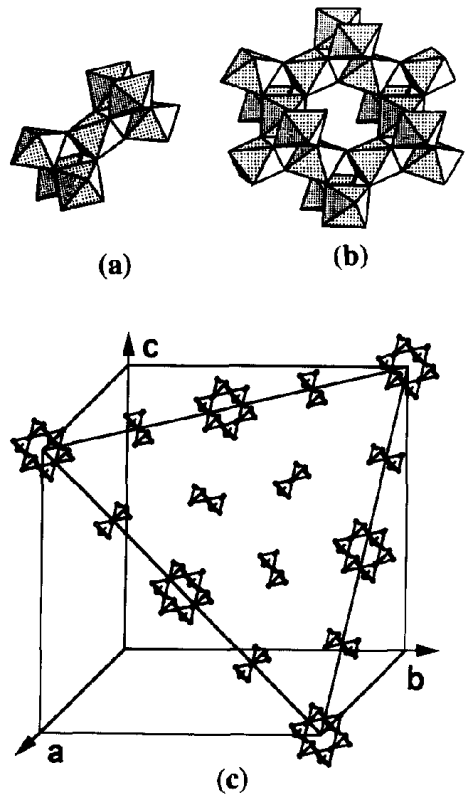

FIG. 2. The Nb–O clusters formed in the type II $Bi_{2-x}Nb_xO_{3+x}$ solid solution, (a) Nb_7O_{30} and (b) $Nb_{18}O_{72}$. (c) Structural model for the type II $Bi_4NbO_{8.5}$, showing the arrangement of the Nb–O clusters in one of the {1 1 1} planes. Only the Nb cations are shown.

higher than that in real space image simulation. A window function can be used to reduce such errors, but at the same time it will significantly reduce the intensities of diffraction maxima far from the center of the SAED patterns, since many Fourier transform operations have to be made in a dynamic calculation. It is more convenient to resolve the problem by choosing carefully the dimensions of the Fourier transform so that the fake periods coincide with those of the stronger sublattice diffraction spots in a pattern. For example, if the sublattice diffraction spots have a period of N in one direction, then a dimension $2N$ or $4N$ or $6N$ . . . ($2N$ multiplied by an integer) would be suitable. In the case of the SAED simulations for $Bi_4NbO_{8.5}$, dimensions of 192 × 128 and 128 × 128 were used for the calculations of the patterns shown in Figs. 1a and 1b, respectively, since the patterns have a 16 × 16 period resulting from the 8 × 8 × 8 superstructure and the presence of a systematically extinct spot between every other sublattice spot.

The second problem of the simulation of SAED patterns arises from an uncertainty of the specimen thickness. In a real pattern, electrons come from a large area, e.g., up to a few μm^2. These electrons are diffracted from different specimen thickness since particles are usually not completely flat, which means that a real diffraction pattern should be a combination of patterns at different specimen thicknesses. Precise intensity of a diffraction peak is also confined by the shape of diffraction spike (specimen shape), and hence a buckled crystal and imprecise orientation will enhance this lack of precision. In addition, the dynamic diffraction process is not exactly described by the multislice approximation for a finite slice thickness, and beam tilting which is not considered here may also affect the intensity of diffraction (17) although by much less than the effects observed in the images, so that the simulated pattern in this way has only a semi-quantitative meaning.

In the present work, using the proposed model described above, two principal SAED patterns of $Bi_4NbO_{8.5}$ in Fig. 1 have been reproduced by the computer simulations with a P factor (threshold coefficient) of 40. Simulated pattern along the [110] direction (Fig. 3a) matches that of Fig. 1a except a few very weak spots such as those with the indices of (1 1 5) and (1 1 11). The simulated SAED pattern along the [100] direction (Fig. 3b) can match the experimental one (Fig. 1b) almost perfectly. Several other models by rearranging the Nb–O clusters according to the symmetries have also been tested and none gave us better results. Therefore, the proposed model shown in Fig. 2 seems to be a good approach to the real structure.

$Bi_{17}Nb_3O_{33}$

Since the contrast of the HREM image fringes on all projections from $Bi_{17}Nb_3O_{33}$ is very weak, it is practically impossible to confirm any model for this structure by computer image simulations. Therefore, simulation of the SAED patterns becomes the only method which we can use to propose a reasonable model for this structure.

The structure of $Bi_{17}Nb_3O_{33}$ is also incommensurate and similar SAED patterns to those of $Bi_4NbO_{8.5}$ have been obtained. One principal pattern along the [110] direction is shown in Fig. 4a. It has been noted that the number of visible satellite diffraction spots on the SAED patterns of the type II $Bi_{2-x}Nb_xO_{3+x}$ solid solution reduced significantly when the content of Nb decreased. On the other hand, careful measurement of the positions of the existing satellite spots indicated that the closest commensurate superunit cell in $Bi_{17}Nb_3O_{33}$ became 11 × 11 × 11 based on δ-Bi_2O_3 instead of 8 × 8 × 8 in $Bi_4NbO_{8.5}$. Hence, 352 × 176 dimensions of Fourier transform were used in the SAED simulations.

To find out possible space groups from the SAED pattern of this structure with such a large unit cell is extremely difficult. A trial and error method was then used to modify the model for $Bi_4NbO_{8.5}$ (Fig. 2) in order to approach the new structure.

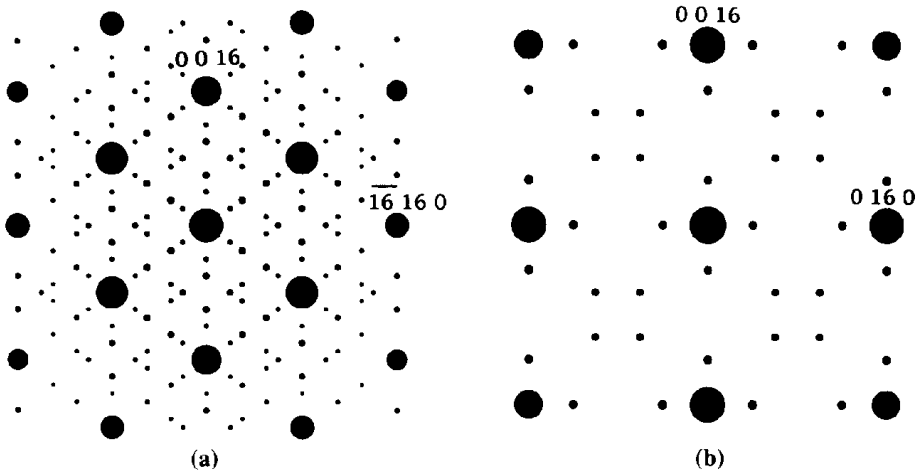

FIG. 3. Computer simulated SAED patterns of $Bi_4NbO_{8.5}$ viewed down the (a) [110] and (b) [100] directions, corresponding to the experimental patterns presented in Fig. 1. The specimen thicknesses used in the simulations are (a) 90 Å and (b) 150 Å. The main diffraction spots are indexed onto the 8 × 8 × 8 supercell.

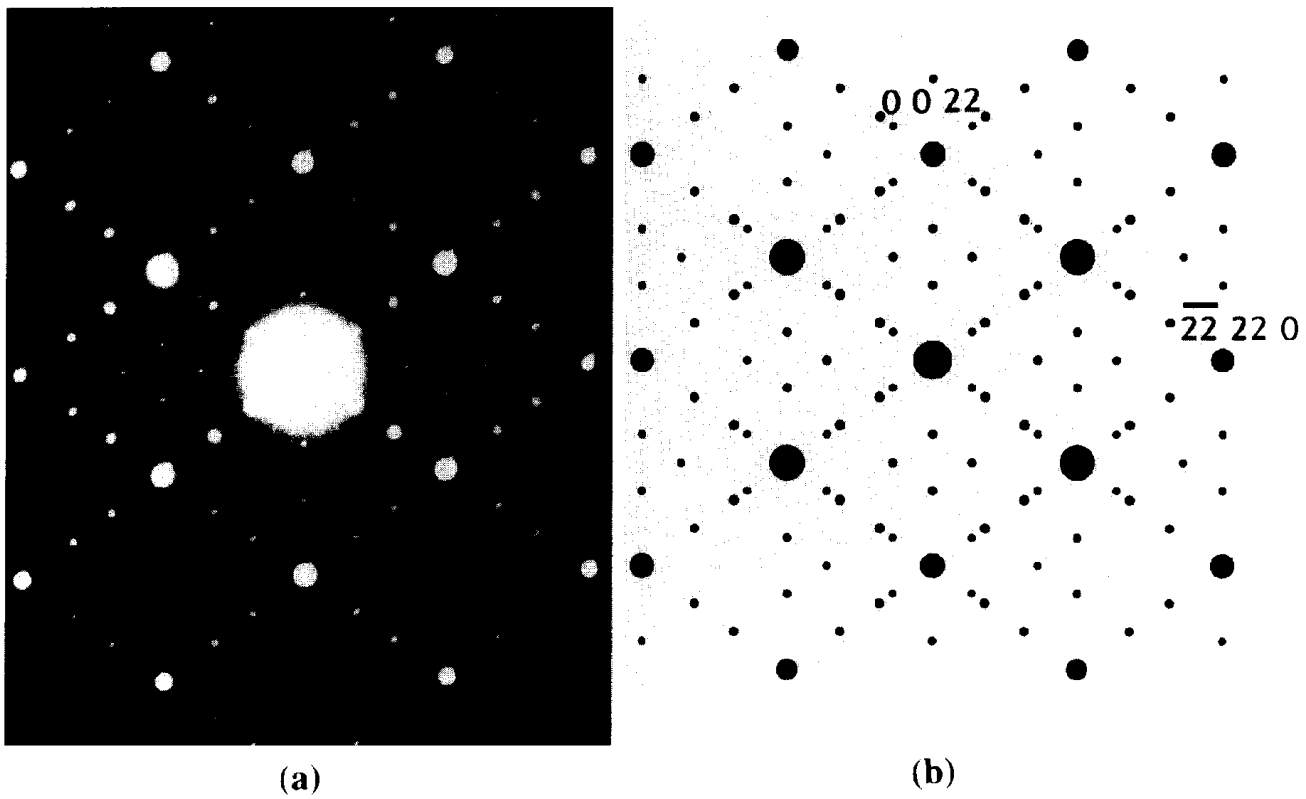

FIG. 4. (a) Experimental SAED pattern of $Bi_{17}Nb_3O_{33}$ viewed down the [110] direction. (b) Simulated pattern corresponding to (a) using an 11 × 11 × 11 superstructural model shown in Fig. 5. The specimen thickness used in the calculation is 108 Å. The *P* factor used is 45.

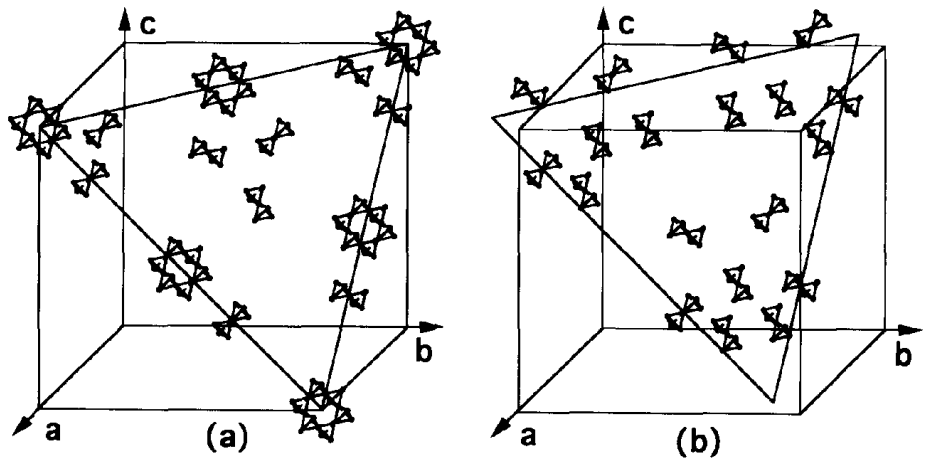

FIG. 5. Schematic drawing of the proposed model for $Bi_{17}Nb_3O_{33}$, showing the arrangement of the Nb–O clusters on (a) one (111) plane and (b) a plane parallel to it with a distance of 3/11 unit cell dimension. Only the Nb cations are shown.

Several points have been found to be very useful in our consideration. First, although the contrast of the HREM image of $Bi_{17}Nb_3O_{33}$ along the [110] direction becomes very weak, a diamond-shaped pattern of the image fringes is still visible, indicating that the Nb–O clusters found in $Bi_4NbO_{8.5}$ perhaps remain in this structure, and they also lie on the {111} planes and possibly other planes parallel to {111} of the 11 × 11 × 11 supercell. Second, the projected structures implied by the SAED patterns along equivalent directions, e.g., [110] and [011], are identical, indicating a cubic symmetry. Finally, the specimen is homogeneous as detected by EDS and XRD, and therefore the composition of the proposed model should be close to $Bi_{17}Nb_3O_{33}$. Based on these considerations, we removed some Nb–O clusters from the model of $Bi_4NbO_{8.5}$ and rearranged the remains in a projected structure in order to obtain the closest diffraction intensities to the observed ones. For example, the intensities of the diffraction peaks of (4 4 4), (7 7 7), (0 0 8), (0 0 16), and (3 3 16), etc., should be significantly stronger than other satellite diffraction peaks, and those of (3 3 3) and (8 8 8) peaks are weak, but still visible (Fig. 4). After obtaining a satisfactory two-dimensionally projected structure, a three-dimensional structure was built up by the combination of several projected structures, and simulations of the SAED patterns along other directions were carried out.

The final model (Fig. 5) has a unit cell composition of $Bi_{4588}Nb_{736}O_{8722}$. The number of the $Nb_{18}O_{72}$ clusters are reduced from the model of $Bi_4NbO_{8.5}$ and some of the $Nb_{18}O_{72}$ clusters are broken up into two Nb_7O_{30} clusters by losing four NbO_6 octahedra. All the Nb–O clusters lie on the {111} planes and some planes parallel to {111}, e.g., a plane with Miller indices (11/8, 11/8, 11/8) in the 11 × 11 × 11 supercell with the dimension of a = 60.5 Å. Using this model, the experimentally observed SAED patterns have been reproduced by computer calculations. As one can see, both positions and intensities of the satellite diffraction spots are matched in a fairly high degree (Fig. 4b).

Bi_9NbO_{16}

From Bi_9NbO_{16}, satellite diffraction spots could only be observed from the ⟨110⟩ directions as shown in Fig. 6a. The superstructure seems to be threefold along the unit cell axes of δ-Bi_2O_3. However, careful measurement reveals that the structure is also incommensurate and the closest commensurate supercell is 11 × 11 × 11 based on δ-Bi_2O_3. Therefore, 352 × 176 Fourier transform dimensions were used in the SAED simulations. Again, it is rather difficult to assume possible space groups for this structure since not enough diffraction spots are visible and the unit cell is too large.

To approach the real structure of Bi_9NbO_{16}, we started from a two-dimensionally projected structure of $Bi_{17}Nb_3O_{33}$ along the [110] direction and further replaced some NbO_6 with Bi–O polyhedra. At its best, the simulated SAED pattern must show strong diffraction spots at (4 4 4), (7 7 7), and the equivalent positions. The intensities of other satellite diffraction spots must be reduced. The final model was achieved by reducing the Nb content to a unit cell composition of $Bi_{4764}Nb_{560}O_{8546}$. A three-dimensional model (Fig. 7) was constructed by combination of several projected structures, in which, all NbO_6 exist in the form of the Nb_7O_{30} clusters. The $Nb_{18}O_{72}$ clusters formerly proposed for the $Bi_{17}Nb_3O_{33}$ structure were either replaced by Bi–O or broken up into two Nb_7O_{30} clusters. Using this model, the experimental SAED pattern of Fig. 6a has been reproduced with all details being matched as shown in Fig. 6b.

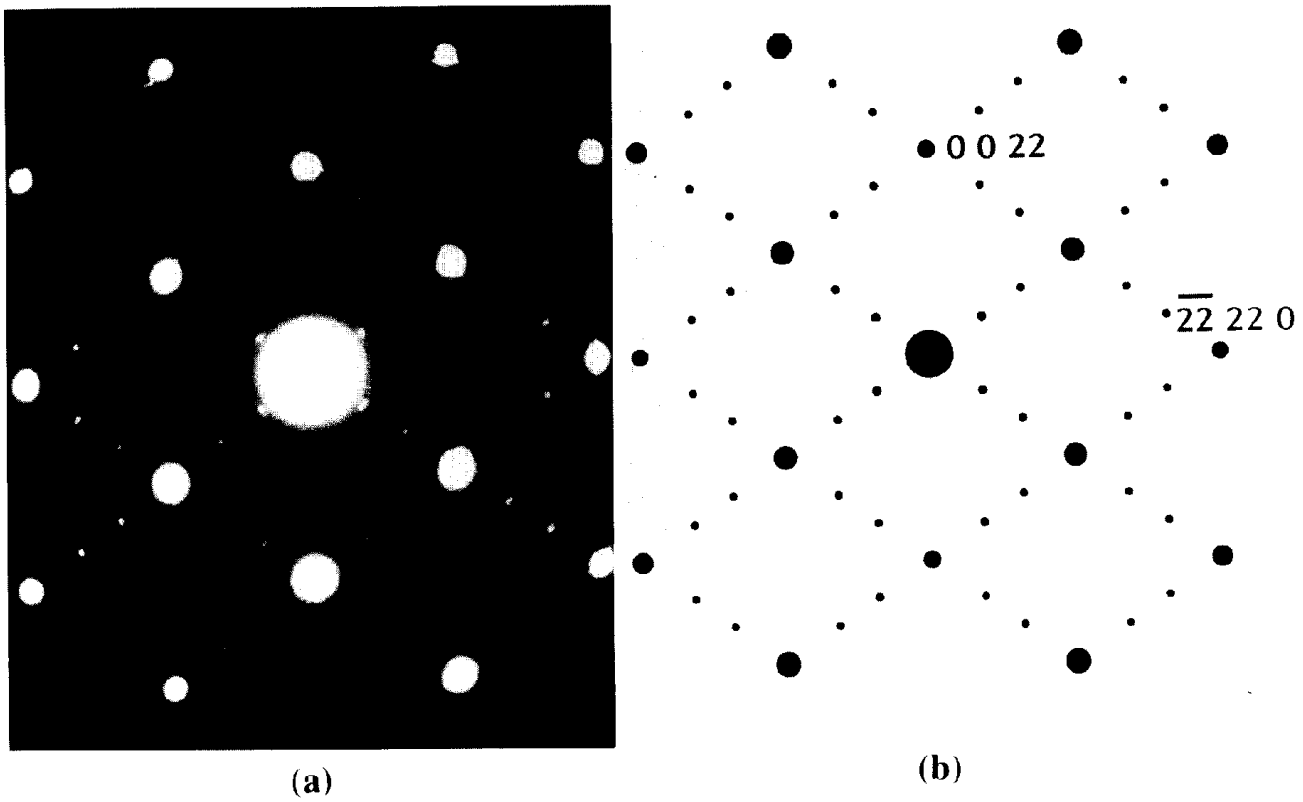

FIG. 6. (a) Experimental SAED pattern of Bi_9NbO_{16} viewed down the [110] direction. (b) Simulated pattern corresponding to (a) using an 11 × 11 × 11 superstructural model shown in Fig. 7. The specimen thickness used in the calculation is 76 Å. The *P* factor used is 50.

The reason for stabilization of the δ-Bi_2O_3 structure at room temperature by adding Nb_2O_5 is that Nb_2O_5 can introduce more oxygen to partially fill the anionic vacancies. In addition, since Nb^{5+} is much smaller than Bi^{3+} and requires octahedral coordination of oxygen, each isolated Nb cation can "freeze" two anionic vacancies in the δ-Bi_2O_3 matrix. The formation of different superstructures is mainly governed by the amount of "active" anionic vacancies. The Nb upper-limit compositions of the type II solid solution therefore depends on the type of the Nb–O clusters, since different forms of the clusters freeze different numbers of anionic vacancies. The formula of

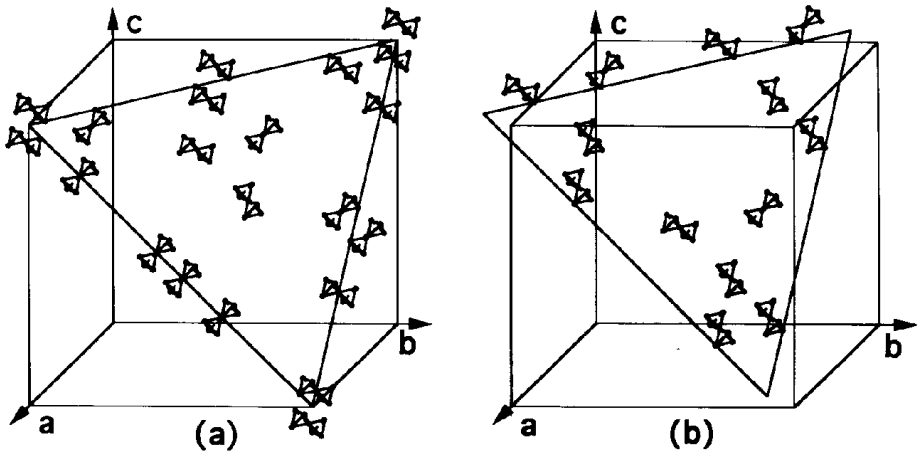

FIG. 7. Schematic drawing of the proposed model for Bi_9NbO_{16}, showing the arrangement of the Nb–O clusters on (a) one (111) plane and (b) a plane parallel to it with a distance of 3/11 unit cell dimension. Only the Nb cations are shown.

the solid solution is $Bi_{2-x}Nb_xO_{3+x}$ with $1 - x$ anionic vacancies. If all the Nb cations form isolated Nb_4O_{18} tetrahedral clusters and all the anionic vacancies are frozen by these clusters, the x value is 4/9, corresponding to a Nb upper-limit composition of $Bi_7Nb_2O_{15.5}$ since each Nb_4O_{18} cluster freezes 5 anionic vacancies. If all the Nb cations exist in the Nb_7O_{30} clusters and each such cluster freezes 8 anionic vacancies, the x value in the Nb upper-limit composition is 7/15, corresponding to a composition of $Bi_{3.28}NbO_{7.42}$. If all the Nb cations are in the $Nb_{18}O_{72}$ clusters and each of these clusters freezes 18 anionic vacancies, the Nb upper-limit composition becomes Bi_3NbO_7. The experimentally observed Nb upper-limit composition for the type II solid solution is between $Bi_{3.28}NbO_{7.42}$ and Bi_3NbO_7. Consequently, the proposed model for $Bi_4NbO_{8.5}$ with a mixture of the Nb_7O_{30} and $Nb_{18}O_{72}$ clusters is reasonable. When the content of Nb reduces, some $Nb_{18}O_{72}$ clusters break up into Nb_7O_{30} clusters, since smaller clusters can freeze relatively more anionic vacancies.

In conclusion, computer simulation of electron diffraction patterns has been used to propose structural models for the type II $Bi_{2-x}Nb_xO_{3+x}$ solid solutions. Although the quality of this technique is by no means as good as the refinements of X-ray or neutronn diffractions, it is so far the only method to resolve the complex structures of the δ-Bi_2O_3-related solid solutions due to its sensitivity to the partial ordering of cations. The real structures of these materials will be eventually approached. In $Bi_4NbO_{8.5}$, the Nb atoms exist in either Nb_7O_{30} or $Nb_{18}O_{72}$ clusters. When the content of Nb reduced, the number of $Nb_{18}O_{72}$ decreased and finally only the Nb_7O_{30} clusters presented in Bi_9NbO_{16}.

Finally, it is worth mentioning that, because of the limited qualitativity of the simulation, the reliability of the method proposed here for structure determination is proportional to the information existing in the diffraction patterns. A large unit cell is an advantage. However, unless the calculation can be done quantitatively in the future, the qualitativity restricts its application to those compounds with superstructures, so that the subcell diffraction spots can be used as reference and only the appearance or extinction of satellite spots are to be matched.

ACKNOWLEDGMENT

The authors thank Dr. D. A. Jefferson for many useful discussions.

REFERENCES

1. H. A. Harwig, *Z. Anorg. Allg. Chem.* **444,** 151 (1978).
2. G. Gattow and D. Schutze, *Z. Anorg. Allg. Chem.* **328,** 44 (1964).
3. T. Takahashi and H. Iwahara, *Mater. Res. Bull.* **13,** 1447 (1978).
4. R. S. Roth and J. L. Waring, *J. Res. Natl. Bur. Stand. Sect. A* **66,** 451 (1962).
5. W. Zhou, D. A. Jefferson, and J. M. Thomas, *Proc. R. Soc. London A* **406,** 173 (1986).
6. W. Zhou, D. A. Jefferson, and J. M. Thomas, *J. Solid State Chem.* **70,** 129 (1987).
7. W. Zhou, D. A. Jefferson, and J. M. Thomas, *Geophys. Monogr.* **45,** 113 (1989).
8. W. Zhou, *J. Solid State Chem.* **76,** 290 (1988).
9. W. Zhou, *J. Solid State Chem.* **101,** 1 (1992).
10. W. Zhou, *J. Solid State Chem.* **108,** 381 (1994).
11. P. R. Buseck, J. M. Cowley, and L. Eyring, *in* "High-Resolution Transmission Electron Microscopy." Oxford Univ. Press, New York, 1988.
12. J. M. Cowley, *in* "Diffraction Physics" 2nd ed. North-Holland, Amsterdam, 1981.
13. J. C. H. Spence, Experimental High Resolution Electron Microscopy. Clarendon, Oxford, 1981.
14. J. E. Wachs, personal communications.
15. O. Savborg and M. Lundberg, *J. Solid State Chem.* **57,** 135 (1985).
16. E. O. Brigham, *in* "The Fast Fourier Transform." Prentice-Hall International, Englewood Cliffs, NJ, 1994.
17. D. J. Smith, L. A. Bursill, and G. J. Wood, *Ultramicroscopy* **16,** 19 (1985).